Tunable multi-window magnomechanically induced transparency; Fano resonances; and slow to fast light conversion

Kamran Ullah,* M. Tahir Naseem, and Özgür E. Müstecaplıoğlu
Department of Physics, Koç University, Sarıyer, İstanbul, 34450, Turkey

We investigate the absorption and transmission properties of a weak probe field under the influence of a strong control field in a hybrid cavity magnomechanical system in the microwave regime. This hybrid system consists of two ferromagnetic material yttrium iron garnet (YIG) spheres strongly coupled to a single cavity mode. In addition to two magnon-induced transparency (MIT) that arise due to strong photon-magnon interactions, we observe a magnomechanically induced transparency (MMIT) due to the presence of nonlinear phonon-magnon interaction. In addition, we discuss the emergence and tunability of the multiple Fano resonances in our system. We find that due to strong photon-magnon coupling the group delay of the probe field can be enhanced significantly. The subluminal or superluminal propagation depends on the frequency of the magnons, which can be easily tuned by an external bias magnetic field. Besides, the group delay of the transmitted field can also be controlled with the control field power.

Keywords: Hybrid magnomechanical system; magnon induced transparency; magnomechanical induced transparency; Fano resonances; subluminal and superluminal effects.

I. INTRODUCTION

Storing information in different frequency modes of light has attracted much attention due to its critical role in high-speed, long-distance quantum communication applications [1–3]. The spectral distinction of optical signals eliminates their unintentional coupling to the stationary information or memory nodes in a communication network. For that aim, multiple transparency window Electromagnetically Induced Transparency (EIT) schemes have been considered for multiband quantum memory implementations mainly in the medium of three-level cold atoms. Experimental demonstrations of three EIT windows have been reported [4], and extended to seven windows using external fields [5]. Observation of nine EIT windows has been experimentally demonstrated quite recently, using an external magnetic field in a vapor cell of Rubidium atoms [6]. A practical question is if such results can be achieved at higher temperatures, for example, for a room temperature multiband quantum memory.

In the last few years, remarkable developments have been achieved to strongly couple spin ensembles to cavity photons, leading to the emerging field of cavity spintronics. Quanta of spin waves, magnons, are highly robust against temperature [7–11], and hence significant magnon-photon hybridization and magnetically induced transparency (MIT) have been successfully demonstrated even at room temperature [11]. Tunable slow light and its conversion to fast light based upon room temperature MIT has been theoretically shown recently [12]. Besides, when coupling of magnons to the thermal vibrations is taken into account in the presence of strong photon-magnon interaction, wide tunability of slow light delay with the applied magnetic field power has been shown [13]. These results demonstrate the promising value of these systems for practical quantum memories [12]. Here we explore how to split such a MIT window into multiple bands for a room temperature multimode quantum memory. Our idea is to exploit the coupling of magnons to thermal vibrations, which is known to yield magnomechanically induced transparency (MMIT) [14], in combination with multiple spin ensembles to achieve multiple bands in MIT. In addition, we discuss the emergence of Fano resonance in the output spectrum and explore the suitable system parameters for its observation. Fano resonance was first reported in the atomic systems [15], and it emerges due to the quantum interference of different transition amplitudes which give minima in the absorption profile. In later years, it has been discussed in different physical systems, such as photonic crystal [16], coupled microresonators [17], optomechanical system [18]. Recently, Fano-like asymmetric shapes have been experimentally reported in a hybrid cavity magnomechanical system [14].

Our model consists of two ferrimagnetic insulators, specifically yttrium iron garnets (YIGs), hosting long-lived magnons at room temperature, placed inside a three-dimensional (3D) microwave cavity; we remark that another equivalent embodiment of our model could be to place the YIGs on top of a superconducting coplanar waveguide, which can have further practical significance being an on-chip device [19]. Specific benefits of YIG as the host of spin ensemble over other systems, such as paramagnetic spin ensembles in nitrogen-vacancy centers is due to its high spin density of 2.1×1022 μB cm^{-3} (μB is the Bohr magneton) and high room temperature spin polarization below the Curie temperature (559 K). In addition to multimode quantum memories, our results can be directly advantageous for readily integrated microwave circuit applications at room temperature such as multimode quantum transducers coupling

*Electronic address: kamran@phys.qau.edu.pk

different systems at different frequencies [20], tunable frequency quantum sensors [21] or fast light enhanced gyroscopes [22]. We will take into account coupling between the magnons and the quanta of YIG lattice vibrations, phonons, arising due to the magnetostrictive force [14], in addition to the magnetic dipole interaction between the cavity field and the spin ensemble. We will only consider the Kittel mode [23] of the ferromagnetic resonance modes of the magnons. Such three-body quantum systems can be of fundamental significance to examine macroscopic quantum phenomena towards thermodynamic limit and quantum to classical transitions [24]. In our work, tunable slow and fast light as a natural consequence of tunable splitting of MIT window will be further examined. The tunability of magnon modes provides the advantage to our system over other reported systems due to high group delays, in the milisec. range, of the transmitted field at room temperature. Slow-light propagation at room temperature has been investigated recently in the cavity magnon-photon system, and the group delays are found to be in the $\sim \mu$s range [12]. In a strongly driven hybrid magnomechanical system, slow-light achieved via MMIT with a maximum group delay of < 0.8 ms [13].

The rest of the paper is organized as follows: We describe the model system in Sec. II and present dynamical equations with steady-state solutions. The results and discussions for MMIT are presented in the Sec. III. We discuss the emergence and tunability of the multiple Fano resonances in Sec. IV. Next, in Sec. V, we present the transmission of the probe field and discuss the group delays for slow and fast light propagation. Finally, in Sec. VI, we present the conclusion of our work.

II. SYSTEM HAMILTONIAN AND THEORY

We consider a hybrid cavity magnomechanical system that consists of two YIGs inside a microwave cavity resonator, as shown in Fig. 1. The presence of uniform bias magnetic fields (z−direction in Fig. 1) excite magnon modes in both YIGs. Due to magnetic dipole interaction, magnon modes are coupled to cavity photons. The excitation of the magnon modes inside the YIG spheres leads to the variation magnetization that results in the deformation of their lattice structure. This deformation forms the vibrational modes (phonons), which couple with the magnons via magnetostrictive interaction [14]. However, we assume that the bias magnetic field on one of the YIG spheres, for example, on the left sphere, is adjusted in such a way that the magnetostrictive interaction can be ignored.

Typically, the magnetostrictive interaction results in a very weak coupling between the magnons and phonons in the range of mHz [14]. To increase this coupling, we consider an additional microwave drive only on the right YIG sphere (YIG2). This external drive also plays the role of a control field in our proposed system. In this

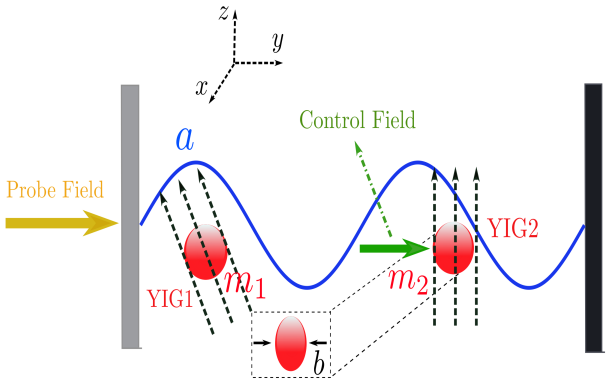

FIG. 1: (color online) The schematic illustration of a hybrid cavity magnomechanical system is shown. It consists of two ferromagnetic Yttrium iron garnet (YIG) spheres placed inside a microwave cavity. Bias magnetic fields are applied in the $z-$direction on both spheres, which excite magnon modes inside them. These magnon modes are strongly coupled with a quantized cavity mode. The bias magnetic field directions are selected in such a way that the phonon mode is excited only in one of the spheres (for example, YIG2) via magnetostrictive interaction. The phonon-magnon interaction strength is typically weak, to enhance this, an external drive magnetic field applied on the YIG2 in $y-$direction, and this drive field also plays the role of the control field. Cavity, phonon, magnon modes of first and second YIGs are represented by a, b, m_1, and m_2, respectively.

work, we consider high quality YIGs each has a diameter 250 μm, composed of ferric ions. The density for ferric ion Fe^{+3} is considered $\rho = 4.22 \times 10^{27} m^{-3}$, which causes the total spin $S = 5/2\rho V_m = 7.07 \times 10^{14}$. Here, V_m is the Volume of the YIG and S is the collective spin operator which satisfy SU(2) Lie algebra i.e., $[S_\alpha, S_\beta] = i\varepsilon^{\alpha\beta\gamma} S_\gamma$. For the interest, the system is probed by a weak probe field. The Hamiltonian of the whole system is given by [23, 24],

$$\begin{aligned} H/\hbar = {} & \omega_a \hat{a}^\dagger \hat{a} + \omega_b \hat{b}^\dagger \hat{b} + \sum_{j=1}^{2} [\omega_j \hat{m}_j^\dagger \hat{m}_j + g_j (\hat{m}_j^\dagger \hat{a} + m_j \hat{a}^\dagger)] \\ & + g_{mb} \hat{m}_2^\dagger \hat{m}_2 (\hat{b} + \hat{b}^\dagger) + i(\Omega_d \hat{m}_2^\dagger e^{-i\omega_d t} - \Omega_d^\star \hat{m}_2 e^{i\omega_d t}) \\ & + i(\hat{a}^\dagger \varepsilon_p e^{-i\omega_p t} - \hat{a} \varepsilon_p^\star e^{i\omega_p t}). \end{aligned} \tag{1}$$

Where $a^\dagger(a)$ and $b^\dagger(b)$ are the creation (annihilation) operators of the cavity and phonon modes, respectively. The resonance frequencies of the cavity, phonon and magnon modes are denoted by ω_a, ω_b and ω_j, respectively. Moreover, m_j is the bosonic operator of the Kittle mode with frequency ω_j and coupling strength g_j with the cavity mode. The frequency ω_j of the magnon mode m_j can be determined by using gyromagnetic ratio γ_j and external bias magnetic field H_j i.e., $\omega_j = \gamma_j H_j$ with $\gamma_j/2\pi = 28$ GHz. The Rabi frequency $\Omega_d = \sqrt{5}/4\gamma\sqrt{N}B_0$ [23], represents the coupling

strength of the drive field with amplitude B_0 and frequency ω_d. Furthermore, in Eq. (1), ω_p is the probe field frequency having amplitude ε_p which can be expressed as; $\varepsilon_p = \sqrt{2P_p\kappa_a/\hbar\omega_p}$. Note that in Eq. (1), we have ignored the non-linear term $K\hat{m}_j^\dagger\hat{m}_j^\dagger\hat{m}_j\hat{m}_j$ that may arise due to strongly driven magnon mode [25, 26]. To ignore this nonlinear term, we must have $K \mid \langle m_2\rangle \mid^3 \ll \Omega$, and for the system parameters we consider in this work, this condition always satisfies. After rotating wave approximation, we can write the modified Hamiltonian of the system

$$\begin{aligned} H/\hbar =&\Delta_a\hat{a}^\dagger\hat{a} + \omega_b\hat{b}^\dagger\hat{b} + \sum_{j=1}^{2}[\Delta_{mj}\hat{m}_j^\dagger\hat{m}_j + g_j(\hat{m}_j^\dagger\hat{a}+ \\ & m_j\hat{a}^\dagger)] + g_{mb}\hat{m}_2^\dagger\hat{m}_2(\hat{b}+\hat{b}^\dagger) + i(\Omega_d\hat{m}_2^\dagger - \Omega_d^\star\hat{m}_2)+ \\ & i(\hat{a}^\dagger\varepsilon_p e^{-i\delta t} - \hat{a}\varepsilon_p^\star e^{i\delta t}). \end{aligned} \tag{2}$$

Here, $\Delta_a = \omega_a - \omega_d$, $\Delta_{mj} = \omega_j - \omega_d$, and $\delta = \omega_p - \omega_d$. The quantum Heisenberg-Langevin equations based on the Hamiltonian in Eq. (2) can be written as

$$\begin{aligned} \dot{\hat{a}} &= -i\Delta_a\hat{a} - i\sum_{j=1}^{2} g_j\hat{m}_j - \kappa_a\hat{a} + \varepsilon_p e^{-i\delta t} + \sqrt{2\kappa_a}\hat{a}^{in}(t), \\ \dot{\hat{b}} &= -i\omega_b\hat{b} - ig_{mb}\hat{m}_2^\dagger\hat{m}_2 - \kappa_b\hat{b} + \sqrt{2\kappa_b}\hat{b}^{in}(t), \\ \dot{\hat{m}}_1 &= -i\Delta_{m1}\hat{m}_1 - ig_1\hat{a} - \kappa_{m1}m_1 + \sqrt{2\kappa_{m1}}\hat{m}_1^{in}(t), \\ \dot{\hat{m}}_2 &= -i\Delta_{m2}\hat{m}_2 - ig_2\hat{a} - \kappa_{m2}m_2 - ig_{mb}\hat{m}_2(\hat{b}+\hat{b}^\dagger) \\ &+ \Omega_d + \sqrt{2\kappa_{m2}}\hat{m}_2^{in}(t). \end{aligned} \tag{3}$$

Where κ_a, κ_b, and $\kappa_{m1}(\kappa_{m2})$ are the decay rates of the cavity, phonon and magnon modes, respectively. Moreover, $\hat{b}^{in}(t)$, $\hat{m}_j^{in}(t)$ and $\hat{a}^{in}(t)$ are the vacuum input noise operators which have zero mean values i.e., $\langle\hat{q_{in}}\rangle = 0$ [27, 28], here, q ϵ a, m, and b. Consequently, we can linearize the quantum Langevin equations and take only the first-order terms in the fluctuating operator: $\left\langle\hat{O}\right\rangle = O_s + \hat{O}_- e^{-i\delta t} + \hat{O}_+ e^{i\delta t}$ [29], here $\hat{O}$ is an arbitrary operator. First, we consider the zero-order solution, namely, steady-state solutions which are given as

$$\begin{aligned} a_s &= -i\sum_{1,2}\frac{g_j m_{js}}{\kappa_a + i\Delta_a}, \\ b_s &= \frac{-ig_{mb}m_{2s}.m_{2s}^\star}{\kappa_b + i\omega_b}, \\ m_{1s} &= \frac{-ig_1 a_s}{\kappa_{m1} + i\Delta_{m1}}, m_{2s} = \frac{\Omega_d - ig_2 a_s}{\kappa_{m2} + i\tilde{\Delta}_{m2}}, \\ \tilde{\Delta}_{m2} &= \Delta_{m2} + g_{mb}(b_s + b_s^\star). \end{aligned} \tag{4}$$

To calculate the optical absorption and transmission of the probe field, we only consider the mean response of the system to weak probe field. Eq. (4) shows that strongly driven magnon mode m_2 results in a large steady-state amplitude $\mid\langle m_{2s}\rangle\mid \gg 1$, and due to beam splitter interaction, this leads to the large steady-state amplitude of the cavity mode $\mid\langle a_s\rangle\mid \gg 1$. In such a situation, the probe field power can be neglected, and only the driving field contribution can be considered. After following some mathematical steps, one can obtain the first-order perturbed solutions of the cavity mode which is given by

$$a_- = \varepsilon_p\left[A' + C_1' + \frac{g_2^2}{\beta'} + \frac{\alpha^\star\alpha'}{\beta^\star\beta' + A^\star - C_1^\star + \frac{g_2^2}{\beta^\star}}\right]^{-1}, \tag{5}$$

where

$$\begin{aligned} A &= \kappa_a + i(\Delta_a + \delta), B = \frac{G_{mb}^2\omega_b}{\omega_b^2 - \delta^2 + i\delta\kappa_b}, \\ C_1 &= \frac{g_1^2}{\kappa_{m1} + i(\Delta_{m1} + \delta)}, C_2 = \frac{g_2^2}{\kappa_{m2} + i(\tilde{\Delta}_{m2} + \delta)}, \\ A' &= \kappa_a + i(\Delta_a - \delta), B' = \frac{G_{mb}^2\omega_b}{\omega_b^2 - \delta^2 - i\delta\kappa_b}, \\ C_1' &= \frac{g_1^2}{\kappa_{m1} + i(\Delta_{m1} - \delta)}, C_2' = \frac{g_2^2}{\kappa_{m2} + i(\tilde{\Delta}_{m2} - \delta)}, \\ \alpha &= \frac{g_2^2 B}{C_2 + iB}, \alpha' = \frac{g_2^2 B'}{C_2' + iB'}, \\ \beta &= C_2 - i\frac{C_2'^\star B}{C_2'^\star + iB}, \beta' = C_2' - i\frac{C_2^\star B'}{C_2^\star + iB'}. \end{aligned}$$

Here $G_{mb} = i\sqrt{2}g_{mb}m_{2s}$ is the effective magnon-phonon coupling. We use the input-output relation for the cavity field $\varepsilon_{out} = \varepsilon_{in} - 2\kappa_a\langle a\rangle$ [30], and the amplitude of the output field corresponding to the input probe field can be written as

$$\varepsilon_{out} = \frac{2\kappa_a a_-}{\varepsilon_p}, x + iy. \tag{6}$$

ε_{out} represents the output field, and it is a complex number in nature with a real part x and imaginary part y. The real and imaginary parts represent the in-phase and out-phase field quadratures corresponding to the probe field. The real part is responsible for the absorption spectrum, whereas the imaginary part attributes to the dispersion spectrum of the output field.

III. MMIT WINDOWS PROFILE

For the numerical calculation, we use parameters from the recently available experiment on the magnon-cavity system unless stated differently [14]. Frequency of the cavity field $\omega_a/2\pi$=10 GHz and its decay rate $\kappa_a/2\pi$=2 MHz, the resonance frequency of the phonon mode is $\omega_b/2\pi$=10 MHz with a decay rate of $\kappa_b/2\pi$=100 Hz. We consider high quality YIG spheres, which consist of ferric ions Fe^{+3} each of diameter d=250 μm and

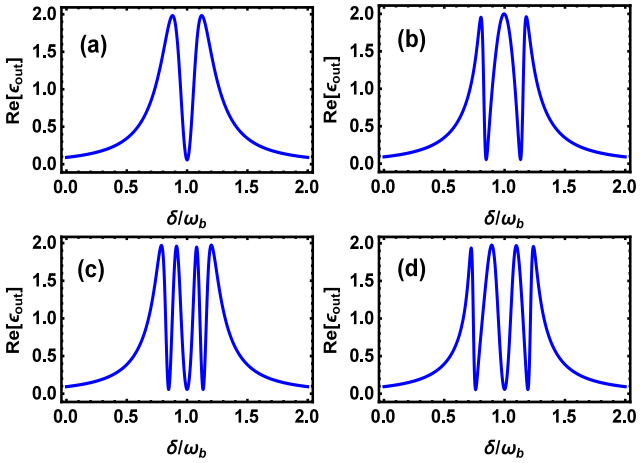

FIG. 2: (Color online). The absorption $Re[\varepsilon_{out-}]$ spectrum of the MIT and MMIT windows profile against the normalized probe field detuning δ/ω_b is plotted for different coupling strengths. (a) $g_1 = g_{mb} = 0$ and $g_2/2\pi = 1.2$ MHz and (b) $g_1 = 0$, $g_2/2\pi = 1.2$ MHz, $G_{mb}/2\pi = 2.0$ MHz (c), (d) $g_1/2\pi = g_2/2\pi = 1.2$ MHz, and (c) $G_{mb}/2\pi = 2$ MHz and (d) $G_{mb}/2\pi = 3.5$ MHz. The other parameters are the same as given in Sec. III.

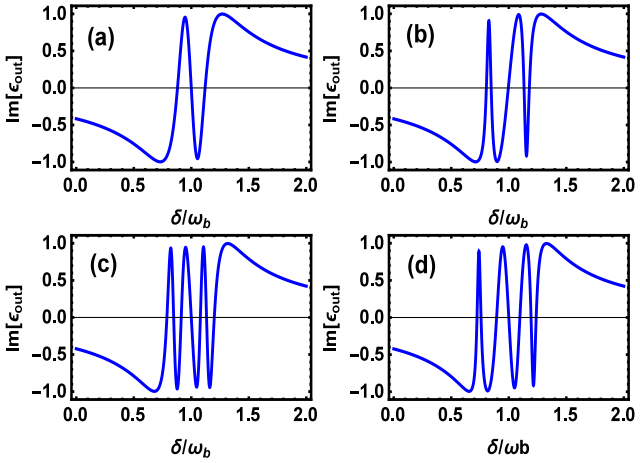

FIG. 3: (Color online) The dispersion $Im[\varepsilon_{out-}]$ spectrum of the MIT and MMIT windows profile against the dimensionless frequency δ/ω_b is shown for different coupling strengths. (a) $g_1 = g_{mb} = 0$ and $g_2/2\pi = 1.2$ MHz and (b) $g_1 = 0$, $g_2/2\pi = 1.2$ MHz, $G_{mb}/2\pi = 2.0$ MHz (c), (d) $g_1/2\pi = g_2/2\pi = 1.2$ MHz, and (c) $G_{mb}/2\pi = 2$ MHz and (d) $G_{mb}/2\pi = 3.5$ MHz. The other parameters are the same as given in Sec. III.

composed of $N = 2.3 \times 10^{16}$ particles. The collective density of each YIG $\rho_j = 4.22 \times 10^{27}\ m^{-3}$ and total spin S=$5/2\rho V_m$=7.07×10^{14}. Moreover, each YIG oscillates with frequency $\omega_{1,2}/2\pi$=10 GHz and have decays $\kappa_{m1}/2\pi = \kappa_{m2}/2\pi$=0.1 MHz. Moreover, YIG2 magnon mode is driven by a microwave field of frequency $\omega_d/2\pi$=10 GHz and associated power is $P = 30$ mW. The magnon-photon couplings are $g_1/2\pi = g_2/2\pi = 1.5$ MHz, and effective magnon-phonon coupling is considered to be $G_{mb}/2\pi = 3.5$ MHz. The detunings are resonant with phonon mode frequency; $\Delta = \omega_b$ and $\Delta_{mj} = \omega_b$.

We will first illustrate the physics behind the multi-band transparency by systematically investigating the role of different couplings in the model. Fig. 2 displays the response of the probe field in the absorption spectrum of the output field for different coupling strengths. In Fig. 2(a), we consider that the magnon mode m_1 coupling with the cavity field is switched-off ($g_1 = 0$), and the magnon-phonon coupling is zero ($g_{mb} = 0$). Consequently, only magnon mode m_2 is coupled with the cavity. In this case, we observe a magnon induced transparency (MIT) in which a typical Lorentzian peak of the output spectrum of the simple cavity splits into two peaks with a single dip, as shown in Fig. 2(a). The width of this transparency window can be controlled via driving field power and the magnon-photon coupling g_2. On increasing the coupling strength g_2 the width of the window increases, and vice versa. Now we consider a case in which g_1 remains zero, however, the coupling of the magnon mode m_2 with the cavity field, and phonon mode is non-zero. Due to the presence of strong magnon-photon coupling g_2, we obtain one MIT, as shown in Fig. 2(b). In addition, the optomechanical-like interaction between the magnon-phonon modes induces a second transparency window, namely magnomechanically induced transparency (MMIT).

To observe MIT in our system, strong magnon-photon coupling ($g_1, g_2 > \kappa_{mj}, \kappa_a, \kappa_b$) is required, the MIT windows disappear in the weak coupling regime. We can observe double MIT by removing magnon-phonon coupling g_{mb}, and considering non-zero couplings between the magnon modes and the cavity field. Finally, if we consider all three couplings simultaneously non-zero, then the transparency window splits into three windows consists of four peaks and three dips, this is shown in Fig. 2(c). In this case, one window is associated with the magnomechanical interaction, and the rest of the two are induced by magnon-photon couplings. The width and peaks separation of these windows increases and broadens, respectively, at higher values of magnon-phonon coupling G_{mb}, which can be seen in Fig. 2(d). Moreover, we have a symmetric multi-window transparency profile where the splitting of the peaks occurs at side-mode frequencies $\omega_p = \omega_b \pm \omega_d$.

In Figs. 3(a-d), we plot the dispersion spectrum of the output field versus normalized frequency of the probe field, for the same cases as shown in Fig. 2. The single MIT dispersion spectrum in the absence of YIG1 and magnon-photon coupling g_{mb} is shown in Fig. 3(a). The dispersion spectra for the case of $g_1 = 0$, $g_2 \neq 0$ and $g_{mb} \neq 0$ is plotted in the Fig. 3(b). In the presence of all three couplings, the dispersion spectrum of the output field is given in the Figs. 3(c-d). It is clear from Figs. 3(c-d), by the increase in the effective magnon-phonon coupling G_{mb}, the transparency windows become wider. We like to point out that the magnomechanically induced amplification (MMIA) of the output field, in our system,

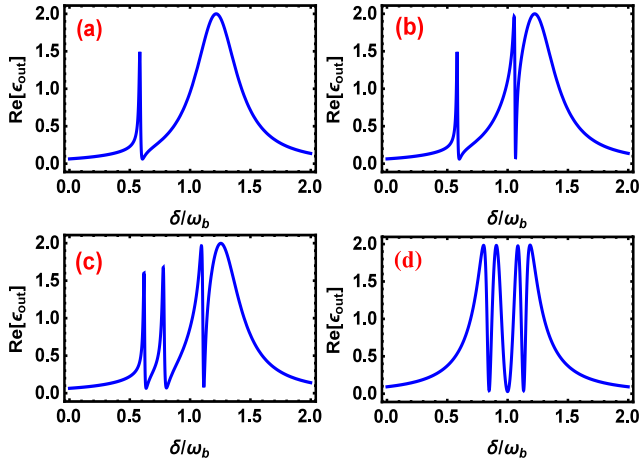

FIG. 4: (Color online) The asymmetric absorption $Re[\varepsilon_{out-}]$ profile of the MIT and MMIT windows profile against the normalized probe frequency δ/ω_b for different cases (a) $\Delta_{m2} = 0.7\omega_b$, $g_2 = 1.5$ MHz, $g_1 = g_{mb} = 0$, and (b) $\Delta_{m2} = 0.7\omega_b$, $g_1 = 0$, $g_2 = 1.5$ MHz, $G_{mb} = 3.5$ MHz, and (c) $\Delta_{m1,2} = 0.7\omega_b$, $g_1 = g_2/2\pi = 1.5$ MHz and $G_{mb}/2\pi = 3.5$MHz (d) $\Delta_{m1,2} = \omega_b$, $g_1 = g_2/2\pi = 1.5$ MHz and $G_{mb}/2\pi = 3.5$ MHz. In all panels, $g_1 = g_2/2\pi = 1.5$ MHz, $G_{mb}/2\pi = 3.5$ MHz, and rest of the parameters are give in Sec. III.

can be obtained in the blue detuned regime; $\Delta_{m2} = -\omega_b$.

IV. FANO RESONANCES IN THE OUTPUT FIELD

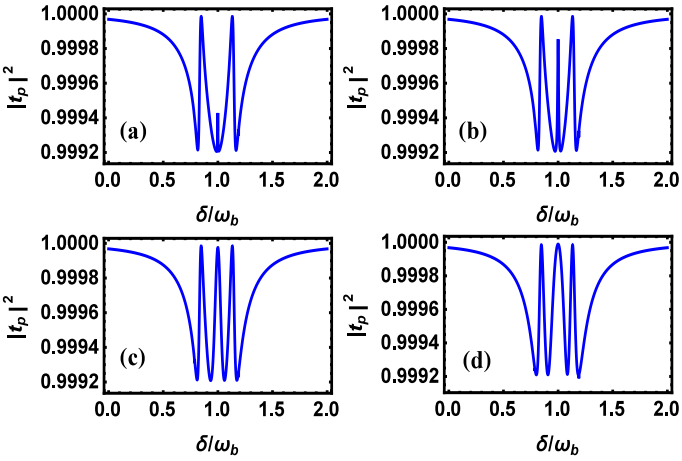

FIG. 5: (Color online). The transmission $|t_p|^2$ spectrum as a function of normalized probe field frequency δ/ω_b is plotted for different values of g_1. (a) $g_1/2\pi = 0.5$ MHz (b) $g_1/2\pi = 0.8$ MHz (c) $g_1/2\pi = 1.2$ MHz (d) $g_1/2\pi = 1.5$ MHz. In all panels, $g_2/2\pi = 1.5$ MHz, $G_{mb}/2\pi = 3.5$ MHz and the other parameters are the same as given in Sec. III.

In the following, we discuss the emergence and physical mechanism of the Fano line shapes in the output spectrum. The shape of the Fano resonance is distinctly different than the symmetric resonance curves in the EIT, MIT, optomechanically induced transparency (OMIT) and MMIT windows [14, 31]. Fano resonance has observed in the systems in which EIT has reported by a suitable selection of the system parameters [14, 31–36]. The physical origin of Fano resonance in the systems having optomechanical-like interactions has explained due to the presence of non-resonant interactions. For example, in a standard optomechanical system, if the anti-Stokes process is not resonant with the cavity frequency, asymmetric Fano shapes appear in the spectrum [31–33]. In our system, this corresponds to $\Delta_{m1} \neq \omega_b$, because instead of a cavity mode, magnon mode m_1 is coupled with phonon mode via optomechanical-like interaction.

We can observe Fano profiles by suitable selection of the system parameters. For this purpose, we suppose that YIG1 has a small mass as compare to YIG2, i.e., $m_2 > m_1$ and oscillates with higher frequency than YIG1 $\omega_2 > \omega_1$. The asymmetric Fano shapes can be seen in Figs. 4(a-c) for different non-resonant cases, where we plot the absorption spectrum of the output field as a function of normalized detuning δ/ω_b. In Fig. 4(a), we consider only non-zero value of the g_2, other two couplings are absent, and the detuning $\Delta_{m2} = 0.7\omega_m$ is non-resonant. The absorption spectrum of the symmetric MIT (Fig. 2(a)) profile changes into asymmetric window profile, as shown in Fig. 4(a). Such asymmetric MIT bands can be related to multiple Fano resonances, emerging frequently in optomechanical systems [31–35]. If we remove the YIG1 and consider the other two couplings g_2 and g_{mb} in the system for $\Delta_{m2} = 0.7\omega_m$, we obtain double Fano resonance in the output spectrum, this is shown in Fig. 4(b). Similarly, in the presence of all three couplings and $\Delta_{m1,m2} = 0.7\omega_m$, the double Fano resonance goes over to a triple Fano resonance, as shown in Fig. 4(c). This is because the cavity field can be build up by three coherent routes provided by the three coupled systems (the magnons, cavity, and phonon modes), and which can interfere with each other. The Fano resonance disappears when we consider the resonance case $\Delta_{m1} = \Delta_{m2} = \omega_b$, as shown in Fig. 4(d).

V. NUMERICAL RESULTS FOR SLOW AND FAST LIGHTS

Here we investigate the transmission and group delay of the output signal in our cavity magnomechanical system. From Eq. (6), the rescaled transmission field corresponding to the probe field can be expressed as

$$t_p = \frac{\varepsilon_p - 2\kappa_a a_-}{\varepsilon_p}. \tag{7}$$

Here, we discuss the transmission spectrum of the probe field and explain the effect of magnon-photon and magnon-phonon couplings on the transmission spectrum. In Figs. 5(a-d), we plot the transmission spectrum of the

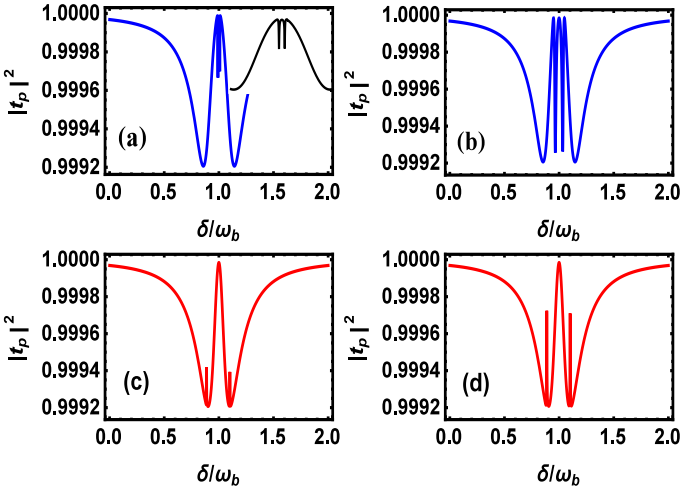

FIG. 6: (Color online). The transmission $|t_p|^2$ spectrum as a function of normalized probe field frequency δ/ω_b is shown for different values of coupling strengths. (a) $G_{mb}/2\pi = 0.5$ MHz (b) $G_{mb}/2\pi = 1.0$ MHz. In (c) and (d), $g_2/2\pi = 0.4$ MHz (d) $g_2/2\pi = 0.8$ MHz. The other parameters are same as in Fig. 5.

probe field against the scaled detuning δ/ω_b, for different values of g_1. It is clear from Fig. 5(a), the transmission peak associated with the magnon-photon coupling of YIG1 is smaller than the other two peaks, for a smaller value of the magnon-photon coupling $g_1/2\pi = 0.5$ MHz. This shows that, in our system, strong magnon-photon coupling ($g_1 \gg \kappa_{m1}$) is required to obtain MIT. By increasing the coupling strength g_1, the peak of the middle transparency profile grows up in height and reaches close to unity, as shown in Figs. 5(b-c). Furthermore, Figs. 5(d) shows that for higher values of the magnon-photon coupling g_1, the middle transparency window becomes broad.

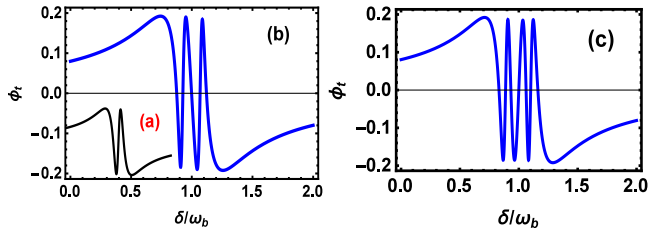

FIG. 7: (Color online) The phase ϕ_t of the transmitted probe field versus normalized detuning δ/ω_b for different coupling strengths. (a) $g_1 = g_{mb} = 0$, (b) $g_1 = 0$, $g_2/2\pi = 1.5$ MHz, $G_{mb}/2\pi = 4$ MHz (c) $g_1/2\pi = g_2/2\pi = 1.5$ MHz, and $G_{mb}/2\pi = 4$ MHz. Rest of parameters are given in Sec. III.

In Figs. 6(a-b), we plot the transmission spectrum of the probe field as a function of dimensionless detuning for different values of G_{mb}. In Figs. 6(a-b), we consider both g_1 and g_2 to be the same in the strong coupling regime. However, the effective coupling $\tilde{g}_2 = g_2\alpha_s$ depends on the steady-state amplitude of the cavity field α_s which depends on the m_{2s}. Consequently, $\tilde{g}_2$ and G_{mb} are related and it can be seen from Eq. (4). For a smaller value of G_{mb} in Fig. 6(a), we have two small peaks associated with g_2 and G_{mb}, in addition, the third-highest peak is associated with g_1. For a fixed value of g_{mb}, if we increase G_{mb}, it increases $\tilde{g}_1$, and the peaks associated with these two couplings become more visible, as shown in Fig. 6(b). Similarly, in Fig. 6(c-d), we observe a similar increase in the height of two peaks associated with g_2 and G_{mb}, for the variation in g_2.

To investigate the phase ϕ_t of the transmitted probe field t_p, we use the relation $\phi_t = \text{Arg}[t_p]$. The plot of the transmitted probe field phase as a function of normalized detuning δ/ω_b for different coupling strengths is shown in Fig. 7. In the inset of Fig. 7(a), we consider both g_1 and g_{mb} are switched off, and only g_2 is present. We obtain the conventional phase of the transmitted field for a single MIT curve, which appears similar to the standard single OMIT case [31]. In Fig. 7(b), we switch-off the YIG1 coupling with the field ($g_1 = 0$), and the other two couplings are present ($g_{mb} \neq 0, g_2 \neq 0$), whereas, in Fig. 7(c), we keep all three couplings in the system. It is clear from Figs. 7(b-c), by introducing additional coupling in such a magnon cavity system, the phase curve of the transmitted probe field splits from single to double and double to triple windows. In Fig. 7(b), we have a MIT and MMIT phase dispersion curves, and in the last case (Fig. 7(c)), we obtain one MMIT and two MIT phase dispersion curves. The transmitted probe field phase is associated with the group delay τ_g of the output field; a more rapid phase dispersion leads to a larger group delays and vice versa. Furthermore, a negative slope of the phase represents a negative group delay or fast light ($\tau_g < 0$) whereas, a positive slope of the transmitted field indicates positive group delay or slow light ($\tau_g > 0$). From Fig. 7, we observe that in the regime of the narrow transparency window, there is a rapid variation in the probe phase, and this rapid phase dispersion leads to a significant group delay.

Fig. 8 shows that the group delay τ_g can be tuned by the variation of the bias magnetic field B_0.

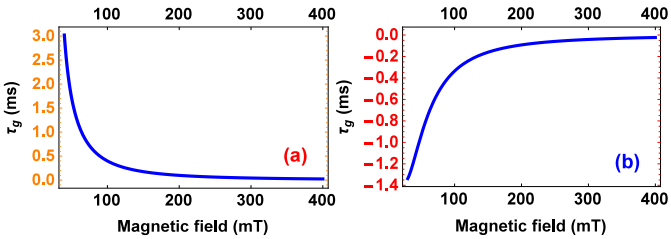

FIG. 8: (Color online) The group delay τ_g of the output probe field against the amplitude of the magnetic field B_0 for (a) $\Delta_{m1} = \omega_b$, and (b) $\Delta_{m1} = -\omega_b$. The other parameter are $\kappa_b/2\pi = 100$ Hz, $2\pi\kappa_{m1} = 2\pi\kappa_{m2} = 0.1$ MHz, $G_{mb}/2\pi = 3.5$ MHz, and $\Omega_d = 1.2 \times 10^{14}$ Hz

The value of the group delay τ_g can be tuned from positive to negative by chaging the detuning $\Delta_{m1} = \omega_b$

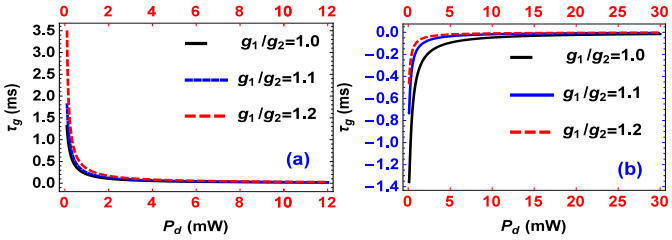

FIG. 9: (Color online) The group delay τ_g of the transmitted probe field as a function of the driving power P_d for several values of the magnon-photon couplings. (a) $\Delta_{m1} = \omega_b$, (b) $\Delta_{m1} = -\omega_b$, and the other parameter are same as given in Fig. 8.

to $\Delta_{m1} = -\omega_b$. We achieve a maximum group delay $\tau_g = 3.0$ ms for slow light propagation for relatively weak magnon-photon couplings $g_1 = g_2 = 0.15\omega_b$ MHz, as shown in Fig. 8(a). Similarly, Fig. 8(b) exhibits fast light propagation against the bias magnetic field in the blue detuned regime $\Delta_{m1} = -\omega_b$, and we observe a maximum group delay of $\tau_g \approx 1.35$ ms. This is one order of magnitude greater than for a magnomechanical system reported in ref. [13].

Finally, we investigate the effect of the magnon-photon couplings on the group delays of the transmitted field. For this purpose, in Figs. 9(a-b), we plot group delays τ against the driving power for different values of the magnon-photon couplings. Fig. 9(a) shows that the magnitude of the group delay increases with the increase in g_1, which indicates that larger group delay can be obtained in the strong magnon-photon coupling regime. Similar results can also be obtained by increasing the magnon-photon coupling g_2. For the blue detuned regime $\Delta_{m1} = -\omega_b$, group delay becomes negative and it increases with the increase in the magnon-photon coupling strength, as shown in Fig. 9(b). Furthermore, we obtain the pulse advancement and delay in the order of $\tau_g = 3.5$ ms and $\tau_g \approx -1.3$ ms, respectively. These can be further enhanced by considering stronger magnon-photon couplings. From Fig. 8 and Fig. 9, we see that the proposed model can be used as a tunable switch, which can be controlled via detuning Δ_{m1}, and our results are comparable with the existing proposals based on the hybrid quantum systems [37–40].

VI. CONCLUSION

We have investigated the transmission and absorption spectrum of a weak probe field under the influence of a strong control field in a hybrid magnomechanical system in the microwave regime. Due to the presence of a nonlinear phonon-magnon interaction, we observed magnomechanically induced transparency (MMIT), and the strong photon-magnon interactions resulted in the magnon induced transparency (MIT). We observed single MMIT, which is a result of the single-phonon process. We find two MIT windows in the output probe spectra due to the presence of two magnon modes coupled with the single cavity mode. This is demonstrated by plotting the absorption, dispersion, and transmission of the output field. We discussed the emergence of Fano resonances in the output field spectrum of the probe field. These asymmetric line shapes appeared due to the presence of anti-Stokes processes in the system. We examined conditions of slow and fast light propagation in our system, which can be controlled by different system parameters. The frequency of the magnons can be tuned with an external bias magnetic field, which provided us with easy tunability of the slow or fast light in the system. Finally, we showed that to achieve long-lived slow light, the control field power should be selected appropriately. Our results suggest that this system may find its applications in the implementation of multi-band quantum memories [12].

Acknowledgment

We Thank Prof. M. Cengiz Onbasli for fruitful discussions. We also thank Prof. Jie Li for his useful comments.

[1] M. Afzelius, C. Simon, H. de Riedmatten, and N. Gisin, Phys. Rev. A **79**, 052329 (2009).
[2] N. Sinclair, E. Saglamyurek, H. Mallahzadeh, J. A. Slater, M. George, R. Ricken, M. P. Hedges, D. Oblak, C. Simon, W. Sohler, and W. Tittel, Phys. Rev. Lett. **113**, 053603 (2014).
[3] P. Jobez, N. Timoney, C. Laplane, J. Etesse, A. Ferrier, P. Goldner, N. Gisin, and M. Afzelius, Phys. Rev. A **93**, 032327 (2016).
[4] D. McGloin, M. H. Dunn, and D. J. Fulton, Phys. Rev. A **62**, 053802 (2000).
[5] K. Ying, Y. Niu, D. Chen, H. Cai, R. Qu, and S. Gong, Journal of Modern Optics **61**, 631 (2014).
[6] S. Bhushan, V. S. Chauhan, D. M, and R. K. Easwaran, Physics Letters A **383**, 125885 (2019).
[7] D. Zhang, X.-M. Wang, T.-F. Li, X.-Q. Luo, W. Wu, F. Nori, and J. You, npj Quantum Information **1**, 1 (2015).
[8] Y. Tabuchi, S. Ishino, T. Ishikawa, R. Yamazaki, K. Usami, and Y. Nakamura, Phys. Rev. Lett. **113**, 083603 (2014).
[9] M. Goryachev, W. G. Farr, D. L. Creedon, Y. Fan, M. Kostylev, and M. E. Tobar, Phys. Rev. Applied **2**, 054002 (2014).
[10] H. Huebl, C. W. Zollitsch, J. Lotze, F. Hocke, M. Greifenstein, A. Marx, R. Gross, and S. T. B. Goennenwein,

Phys. Rev. Lett. **111**, 127003 (2013).
[11] X. Zhang, C.-L. Zou, L. Jiang, and H. X. Tang, Phys. Rev. Lett. **113**, 156401 (2014).
[12] Z. Liu, H. Xiong, and Y. Wu, IEEE Access **7**, 57047 (2019).
[13] C. Kong, B. Wang, Z.-X. Liu, H. Xiong, and Y. Wu, Opt. Express **27**, 5544 (2019).
[14] X. Zhang, C.-L. Zou, L. Jiang, and H. X. Tang, Science Advances **2** (2016), 10.1126/sciadv.1501286.
[15] U. Fano, Phys. Rev. **124**, 1866 (1961).
[16] M. V. Rybin, A. B. Khanikaev, M. Inoue, K. B. Samusev, M. J. Steel, G. Yushin, and M. F. Limonov, Phys. Rev. Lett. **103**, 023901 (2009).
[17] Y.-F. Xiao, M. Li, Y.-C. Liu, Y. Li, X. Sun, and Q. Gong, Phys. Rev. A **82**, 065804 (2010).
[18] S. Kaur, B. Yao, Y.-S. Gui, and C.-M. Hu, Journal of Physics D: Applied Physics **49**, 475103 (2016).
[19] R. Hisatomi, A. Osada, Y. Tabuchi, T. Ishikawa, A. Noguchi, R. Yamazaki, K. Usami, and Y. Nakamura, Phys. Rev. B **93**, 174427 (2016).
[20] N.-H. Kim, J. Jung, J. Cho, D.-S. Han, Y. Yin, J.-S. Kim, H. J. M. Swagten, and C.-Y. You, Applied Physics Letters **108**, 142406 (2016), https://doi.org/10.1063/1.4945685 .
[21] M. Huang, Y. Zhang, F. Li, L. Zhang, R. S. Ruoff, Z. Wen, and Q. Liu, Scientific reports **4**, 3878 (2014).
[22] C. Kittel, Phys. Rev. **73**, 155 (1948).
[23] J. Li, S.-Y. Zhu, and G. S. Agarwal, Phys. Rev. Lett. **121**, 203601 (2018).
[24] J. Li and S.-Y. Zhu, New Journal of Physics **21**, 085001 (2019).
[25] Y.-P. Wang, G.-Q. Zhang, D. Zhang, X.-Q. Luo, W. Xiong, S.-P. Wang, T.-F. Li, C.-M. Hu, and J. Q. You, Phys. Rev. B **94**, 224410 (2016).
[26] Y.-P. Wang, G.-Q. Zhang, D. Zhang, T.-F. Li, C.-M. Hu, and J. Q. You, Phys. Rev. Lett. **120**, 057202 (2018).
[27] H. Xiong and Y. Wu, Applied Physics Reviews **5**, 031305 (2018), https://doi.org/10.1063/1.5027122 .
[28] M. Aspelmeyer, T. J. Kippenberg, and F. Marquardt, Reviews of Modern Physics **86**, 1391 (2014).
[29] S. Huang and G. S. Agarwal, Phys. Rev. A **83**, 043826 (2011).
[30] C. Gardiner, P. Zoller, and P. Zoller, *Quantum noise: a handbook of Markovian and non-Markovian quantum stochastic methods with applications to quantum optics* (Springer Science & Business Media, 2004).
[31] K. Qu and G. S. Agarwal, Phys. Rev. A **87**, 063813 (2013).
[32] K. Ullah, H. Jing, and F. Saif, Phys. Rev. A **97**, 033812 (2018).
[33] K. Ullah, Eur. Phys. J. D **73**, 267 (2019).
[34] K. A. Yasir and W.-M. Liu, Scientific reports **6**, 22651 (2016).
[35] M. J. Akram, F. Ghafoor, and F. Saif, Journal of Physics B: Atomic, Molecular and Optical Physics **48**
[36] S. Zhang, J. Li, R. Yu, W. Wang, and Y. Wu, Scientific reports **7**, 1 (2017).
[37] C. Genes, D. Vitali, and P. Tombesi, Phys. Rev. A **77**, 050307 (2008).
[38] K. Ullah, Chinese Physics B **28**, 114209 (2019).
[39] D. Tarhan, S. Huang, and O. E. Müstecaplıoğlu, Phys. Rev. A **87**, 013824 (2013).
[40] F. Saif, K. Ullah, and S. Watanabe, AIP Conference Proceedings **2067**, 020002 (2019).